

A Novel Analytical Method for Contact Stress of Flexible Joint in Ultra-short-radius Drilling Tools

Xiuxing Zhu^{1,*}, Yingpeng Xu¹, Xiaoyang Li², Rui Hou³ and Guigen Ye^{1,4}

¹College of Pipeline and Civil Engineering, China University of Petroleum (East China), Qingdao 266580, China

²CNPC Tianjin Bo-Xing Engineering Science & Technology Co. Ltd., Tianjin 300451, China

³CNPC Changqing Oilfield Company Natural Gas Evaluation Project Department, Qingyang 745000, China

⁴Delft University of Technology, Mekelweg 4 2628 CD Delft, Netherland

Received 12 August 2022; Accepted 6 December 2022

Abstract

The contact stress of flexible joint is an important factor affecting the safety of ultra-short-radius drilling tools. However, calculating the contact stress accurately is difficult, because the method for solving the multibody collision of the flexible joint is complex. A novel analytical method for the contact stress of ball cage flexible joint is presented in this study. The method was used to establish the relationship between the parameters and contact stress of the flexible joint during the drilling process. The contact stress analytical models of the ball head, ball key, and ball seat were established based on Hertz contact theory, and the finite element method was used to analyse the variations of contact stress under the weight of bit and torque. The influences of borehole curvature and deflection angle on contact stress were discussed for parameter optimization. Results demonstrate that the contact stress values on the ball key, inner raceway, and outer raceway are concentrative. The ball key is the most dangerous part of the flexible joint, and its safety can be improved by increasing its diameter. When the deflection angle between the flexible joint was increased from 0 ° to 18 °, the contact stress value also increased to 220 MPa. However, the contact position was random on the inside of deflection. The proposed method provides a good prospect to optimize the structure parameters of the flexible joint and ultra-short-radius drilling parameters.

Keywords: Ball cage flexible joint, Ultra-short radius drilling tools, Hertz contact theory, Contact stress, Safety evaluation

1. Introduction

Ultra-short-radius horizontal well is a low-cost and high-benefit production technology for remaining oil, which is different from conventional horizontal well. Its curvature radius is small and not more than 4 m, thus, conventional drilling tools cannot meet the drilling requirement. Special flexible drilling tools need to be developed. At present, ultra-short-radius horizontal wells have been widely used in the oilfield. Flexible drilling tools are the key parts and are composed of a guide pipe, a flexible drill pipe, and a bit. The flexible drill pipe is hinged by multiple flexible joints and can pass through a curved wellbore with a small curvature radius. At present, different types of flexible drill pipes have been developed. Hill [1] developed an improved drill string component that can bend pipes with a radius as short as 25–50 feet in the well. Luo [2] established a model of hinged flexible pipe and studied the dynamic characteristics under different constraints. Warren [3] developed a short-radius drilling system composed of a bit, a flexible joint, a sliding sleeve, an indicator, and a flexible drill string, which greatly increased the production. The cross-axis universal joint was used in three types of flexible joint and has the advantages of simple structure and high efficiency, but it also has some disadvantages, such as limited swing angle (less than 25 °), large friction force, and large energy loss.

During the process of ultra-short-radius drilling, the

flexible joint produces contact stress under the weight of bit (WOB) and torque, which reduces the structural strength of drilling tools. Therefore, studying the relationship between flexible joint parameters and contact stress is important. From which, we can optimize parameters and reduce contact stress to ensure the safety of drilling tools. However, multibody collision contact will be produced between the ball cage flexible joints, which is a complex nonlinear problem and is difficult to study.

Scholars all over the world have conducted several research studies on the collision contact of universal joints [5–8], but an analytical method considering the influence of drilling loads and deflection angle has not yet been proposed. Therefore, establishing a method for multibody collision contact stress and optimizing the parameters of a flexible joint are urgently needed.

Based on the above analysis, this study establishes the contact stress analytical method of ultra-short radius flexible joint. Subsequently, the variation of contact stress is studied, and the relationship between flexible joint parameters and contact stress is developed. The proposed method provides a good prospect to optimize the structure parameters of flexible joint and ultra-short radius drilling parameters.

2. State of the art

Scholars have conducted much research on the contact model of ball cage universal joint used in the automobile industry and robot industry. Anoopnath [5] calculated the

*E-mail address: zhuxx99@126.com

ISSN: 1791-2377 © 2022 School of Science, IHU. All rights reserved.

doi:10.25103/jestr.156.22

maximum contact pressure between the deep groove ball bearing and the inner race and compared the calculated results. The results were used to predict the contact pressure between the inner race and the ball, but the model is relatively simple. Pandiyarajan [6] and Virendra [7] used Hertz elliptical contact theory to determine the maximum contact pressure of large-diameter ball bearings and compared it with the contact stress obtained by finite element method, but the author did not study the influence of rotational speed and other factors. Louay [8] studied the contact stress of pear cam mechanism. The effect of contact compression load on the contact stress distribution of the cam profile at contact point was studied. Numerical simulation was performed using the FEM software, and contact stress was determined. Based on Hertz contact theory, this research method was aimed at the cam structure and was not completely applicable to the ball cage universal joint. Zhao [9] proposed a fast method for calculating the contact stress distribution and contact radius in the elastic-plastic contact between two spheres. The proposed fast-solving method can be applied to perform elastic-plastic contact analysis in engineering practice. Molla [10] evolved the equivalent mechanical load of the wheel by finite element analysis, and the values obtained by FEA and Hertz theory were matched, but this method made several assumptions about the model, which affected the calculation accuracy. Luo [2,11,12] combined 3-D beam elements, universal joint elements, rigid beam elements, and beam-beam contact elements to establish a two-layer contact nonlinear finite element model of the flexible drilling tool in the wellbore. The dynamic relaxation method was introduced for numerical solution. The mechanical analysis of flexible drilling tool under the four-hole inclinations in the oblique section was carried out, but the model adopts the cross-shaft universal joint. Therefore, the method can be used for reference, but the model needs to be further modified. Osvaldo [13] proposed a new approach to describe 2D frictional contact problems based on the use of coupling finite elements and a combined contact/friction damage constitutive mode, but the gap between multi-bodies was not considered in this method. Liu [14] analyzed the first titanium alloy drill pipe failure accident that occurred during the drilling of an ultra-short-radius horizontal well in China and conducted physical and chemical analyses, microstructure observation, scanning electron microscopy, and full-scale torsion tests, but did not give the specific calculation method of contact stress. Zhang [15] and Bautista [16] used parametric design technology to establish a standard parts model library of ball cage constant-velocity universal joint. They also developed a 3D parametric design system. Static calculation of the automatically generated parts was performed. However, the research adopted the method of static analysis, and the result error of contact stress was large. Paul [17] and Ian [18] developed a multibody analysis simulation model for ball-type CVJ and compared the numerical results with the analytical results in the case of static non-deflection joints to verify the correctness of the model, but the model does not consider the influence of deflection angle. Simpson [19] and Rebecca [20] developed an existing mathematical model for the case of cross-groove CVJs, including an accurate contact mechanics model. The improved model shows the correlations between predicted contact force variation and wear scar depths during ball reversals but does not analyze the relationship between contact stress and structural parameters.

The above studies are mainly aimed at the contact stress of the single ball cage flexible joint, and there are few studies considering borehole curvature and drilling load. Hence, the study proposes a novel analytical method for contact stress of ball cage flexible joint. The method is based on the Hertz contact theory. The contact stress between the ball key, the inner and outer raceway are studied by the approach. The finite element method was used to study the variation of contact stress under the weight of bit and torque, and the strength of flexible joint is discussed.

The remainder of this study is organized as follows. Section 3 establishes the contact stress model according to Hertz contact theory. Section 4 discusses the variation of contact force on the flexible joint. Section 5 summarizes the conclusions.

3. Contact stress model of flexible joint

Our team developed a ball cage flexible joint [4] as shown in Fig. 1 to overcome the above problems. The most important part of the flexible drill pipe is the ball cage flexible joint, which is composed of a ball head, a ball cage, ball keys, and a ball seat. The outer surface of the ball head of the ball cage flexible joint has six arc grooves as the inner raceway of the ball key. The six arc grooves corresponding to the inner surface of the ball seat are the outer raceway of the ball key, and the ball key in the raceway is installed in the square hole of the ball cage to constrain six steel balls in the same motion plane. The drilling torque is input by the ball head and output by the ball key and ball seat to drive the rotation of the flexible drill rod.

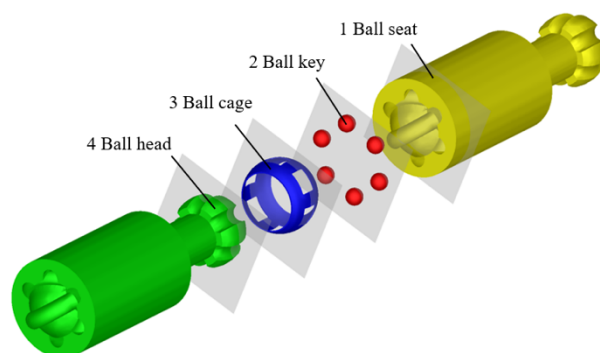


Fig. 1. Structure diagram of ball cage flexible joint

Fig. 2 shows the structure of ball key. The section shape of raceway is oval and its parameters are shown in Table 1.

Table 1. Parameters of flexible joint

Maximum torque	Radius of the distribution ball key	Diameter of the ball key	Pressure angle
1800 kN.m	32 mm	7.5 mm	45 °

Assuming that the forces acting on each ball key are equal under ideal conditions, and the direction of the circumferential force F is the tangent direction of the ball key distribution circle. Since the pressure angle β between the ball key and the contact point is 45 °, and the six ball keys bear the same load when the torque is transferred, the normal pressure acting on the contact point of the ball key and the raceway is:

$$P = \frac{M_{\max}}{6R \cos \beta} = \frac{M_{\max}}{6R \cos 45^\circ} = 13258.3N \quad (1)$$

Where, M_{max} is the maximum transmitted torque, and R is the radius of the distribution ball key circle.

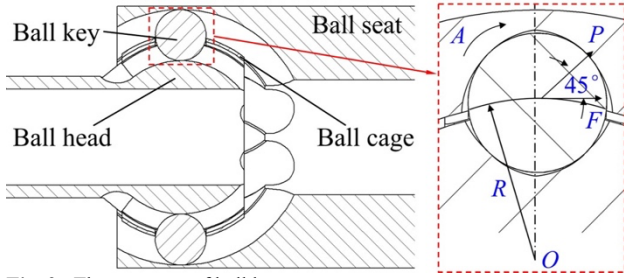


Fig. 2. The structure of ball key

The ball cage flexible joint raceway is a variable curvature ellipse. Considering the curvature of the raceway changes only 5% along the axis of the contact ellipse, the curvature of the whole contact area can be approximately regarded as equal. The radius of curvature is approximately 1.03 to 1.05 times the diameter of the ball key. Assuming that the contact stress is elastic, and the contact surface is much smaller than the curvature radius of the contact point, the contact stress can be solved using Hertz theory directly.

Fig. 3 shows a principal curvature diagram of the inner ball head raceway, when it is in contact with the ball key.

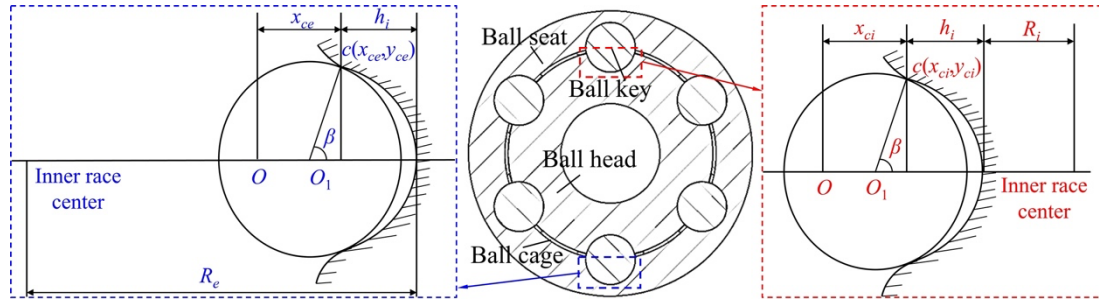


Fig. 3. The contact model between the head seat and the ball key

Similarly, the ball key contact radius of principal curvature R_1 and equivalent radius of curvature R_1' are:

$$R_1 = R_1' = \frac{d}{2} = 7.5mm \quad (5)$$

The main curvature radius R_2 of the ball seat contact is:

$$R_2 = -1.04R_1 = -7.8mm \quad (6)$$

The ball seat equivalent radius of curvature R_2' is:

$$R_2' = -R_e + R_e = -R_e + \frac{\sqrt{2f_e} \sin^2 \beta}{1 + \sqrt{2f_e} \cos \beta} \cdot \frac{d}{2} = -31.8mm \quad (7)$$

Where, R_e is the ball seat radius of raceway bottom, and its value is 34 mm. f_e is the instantaneous curvature coefficient of the ball seat outer raceway, and its value is 0.52. Other parameters have the same meaning as above.

The radius of principal curvature R_1 and the equivalent radius of curvature R_1' are:

$$R_1 = R_1' = \frac{d}{2} = 7.5mm \quad (2)$$

Where, d is the diameter of the ball key, and its unit is mm.

The ball head contact radius R_2 of the main curvature is:

$$R_2 = -1.04R_1 = -7.8mm \quad (3)$$

The ball head equivalent radius of curvature R_2' is:

$$R_2' = R_i + R_h = R_i + \frac{\sqrt{2f_i} \sin^2 \beta}{1 + \sqrt{2f_i} \cos \beta} \cdot \frac{d}{2} = 20.2mm \quad (4)$$

Where, R_i is the bottom radius of the outer ball head raceway, and its value is 18 mm. f_i is the instantaneous curvature coefficient of raceway, and its value is 0.52. β is the pressure angle of the ball cage flexible joint, and its value is 45°.

As shown in Fig. 3, the contact surface formed by two objects under the action of normal force P is an ellipse, and the long and short semi-axes of the contact ellipse are:

$$a' = \alpha \cdot \sqrt{\frac{1 - \lambda_1^2}{E_1} + \frac{1 - \lambda_2^2}{E_2}} \cdot \frac{3P}{2 \cdot \left(\frac{1}{R_1} + \frac{1}{R_1'} + \frac{1}{R_2} + \frac{1}{R_2'} \right)} \quad (8)$$

$$b' = \beta \cdot \sqrt{\frac{1 - \lambda_1^2}{E_1} + \frac{1 - \lambda_2^2}{E_2}} \cdot \frac{3P}{2 \cdot \left(\frac{1}{R_1} + \frac{1}{R_1'} + \frac{1}{R_2} + \frac{1}{R_2'} \right)} \quad (9)$$

Where, λ_1 and λ_2 are Poisson's ratios of the two contacts. E_1 and E_2 are the elastic modulus of the two contacts. R_1 and R_1' are the radius of principal curvature and equivalent radius of the ball head surface at the contact point. R_2 and R_2' are the radius of principal curvature and equivalent radius of the ball head at the point of contact.

$$A = \frac{1}{2} \left[\left(\frac{1}{R_1} - \frac{1}{R_1'} \right)^2 + \left(\frac{1}{R_2} - \frac{1}{R_2'} \right)^2 + 2 \left(\frac{1}{R_1} - \frac{1}{R_1'} \right) \times \left(\frac{1}{R_2} - \frac{1}{R_2'} \right) \cos 2\psi \right]^{\frac{1}{2}} \quad (10)$$

$$B = \frac{1}{2} \left(\frac{1}{R_1} + \frac{1}{R_1'} + \frac{1}{R_2} + \frac{1}{R_2'} \right) \quad (11)$$

Where, ψ is the angle between the plane where the two main radius of curvature R_1 and R_2 exist. α and β depend on the ratio of A to B , and the relationship between α , β and A/B is shown in Table 2.

Table 2. The relationship between α , β and A/B

A/B	0.10	0.20	0.30	0.40	0.50	0.60	0.70	0.80	0.90	0.94	0.99
α	1.070	1.150	1.242	1.351	1.486	1.661	1.905	2.292	3.093	3.824	7.774
β	0.936	0.878	0.822	0.769	0.717	0.664	0.608	0.544	0.461	0.412	0.287

The equation (2)-(4) are substituted into the equation (10)-(11) respectively to obtain:

$$A = \frac{1}{2} \left[\left(\frac{1}{R_1} - \frac{1}{R_1'} \right)^2 + \left(\frac{1}{R_2} - \frac{1}{R_2'} \right)^2 + 2 \left(\frac{1}{R_1} - \frac{1}{R_1'} \right) \times \left(\frac{1}{R_2} - \frac{1}{R_2'} \right) \cos 2\psi \right]^{\frac{1}{2}} = 0.0889 \text{mm}^{-1} \quad (12)$$

$$B = \frac{1}{2} \left(\frac{1}{R_1} + \frac{1}{R_1'} + \frac{1}{R_2} + \frac{1}{R_2'} \right) = 0.0940 \text{mm}^{-1} \quad (13)$$

$$A/B = 0.95 \quad (14)$$

Where, $\alpha=4.166$ and $\beta=0.395$ are obtained from Table 2 by interpolation method.

In this study, the materials used for the ball-cage flexible joint excerpt are 35CrMo, the elastic modulus is 210 GPa, and Poisson's ratio is 0.3. According to the formula, the length of the contact ellipse of the ball head can be obtained as follows:

$$a' = \alpha \cdot \sqrt{\frac{3P}{2} \cdot \frac{\frac{1-\lambda_1^2}{E_1} + \frac{1-\lambda_2^2}{E_2}}{\frac{1}{R_1} + \frac{1}{R_1'} + \frac{1}{R_2} + \frac{1}{R_2'}}}} = 4.052 \text{mm} \quad (15)$$

$$A = \frac{1}{2} \left[\left(\frac{1}{R_1} - \frac{1}{R_1'} \right)^2 + \left(\frac{1}{R_2} - \frac{1}{R_2'} \right)^2 + 2 \left(\frac{1}{R_1} - \frac{1}{R_1'} \right) \times \left(\frac{1}{R_2} - \frac{1}{R_2'} \right) \cos 2\psi \right]^{\frac{1}{2}} = 0.0484 \text{mm}^{-1} \quad (18)$$

$$B = \frac{1}{2} \left(\frac{1}{R_1} + \frac{1}{R_1'} + \frac{1}{R_2} + \frac{1}{R_2'} \right) = 0.0535 \text{mm}^{-1} \quad (19)$$

$$A/B = 0.90 \quad (20)$$

It is obtained from Table 2 by interpolation method: $\alpha=3.093$, $\beta=0.461$.

According to the formula, the length of the contact ellipse of the ball seat and the half-axis length are respectively:

$$a' = \alpha \cdot \sqrt{\frac{3P}{2} \cdot \frac{\frac{1-\lambda_1^2}{E_1} + \frac{1-\lambda_2^2}{E_2}}{\frac{1}{R_1} + \frac{1}{R_1'} + \frac{1}{R_2} + \frac{1}{R_2'}}}} = 3.008 \text{mm} \quad (21)$$

$$b' = \beta \cdot \sqrt{\frac{3P}{2} \cdot \frac{\frac{1-\lambda_1^2}{E_1} + \frac{1-\lambda_2^2}{E_2}}{\frac{1}{R_1} + \frac{1}{R_1'} + \frac{1}{R_2} + \frac{1}{R_2'}}}} = 0.384 \text{mm} \quad (16)$$

The maximum contact stress value of the ball head is:

$$\sigma_{\max} = \frac{3}{2} \cdot \frac{P}{\pi a' b'} = 4068.4 \text{MPa} \quad (17)$$

Substitute the equation (5)-(7) into the equation (10)-(11) respectively, then we can obtain:

$$b' = \beta \cdot \sqrt{\frac{3P}{2} \cdot \frac{\frac{1-\lambda_1^2}{E_1} + \frac{1-\lambda_2^2}{E_2}}{\frac{1}{R_1} + \frac{1}{R_1'} + \frac{1}{R_2} + \frac{1}{R_2'}}}} = 0.448 \text{mm} \quad (22)$$

The maximum stress value of the tee contact surface is:

$$\sigma_{\max} = \frac{3}{2} \cdot \frac{P}{\pi a' b'} = 4697.6 \text{MPa} \quad (23)$$

In the actual construction process, the axial force of the flexible joint is small, and the contact stress generated by the axial stress is also small. So, it's negligible.

4. Result Analysis and Discussion

Fig. 4 shows the structure of ultra-short radius flexible joint. The material is 35CrMo, and the specific material parameters are shown in Table 3.

The ball cage flexible joint contains a total of 20 contact pairs, and each part is shown in Fig. 5 during the working process, the ball key mainly makes rolling and sliding movement in the inner and outer raceway. The ball key is set

as the contact body, meanwhile the ball head and ball seat are set as the target body. According to the working state of the flexible joint, a fixed constraint is imposed on one end of the flexible joint ball head, and a torque (the value is 1.8 kN.m) is applied on one end of the ball seat. Considering that the flexible joint will collide with the guide tube in the process of motion, an axial force of 1000 N is applied at the end of the ball seat.

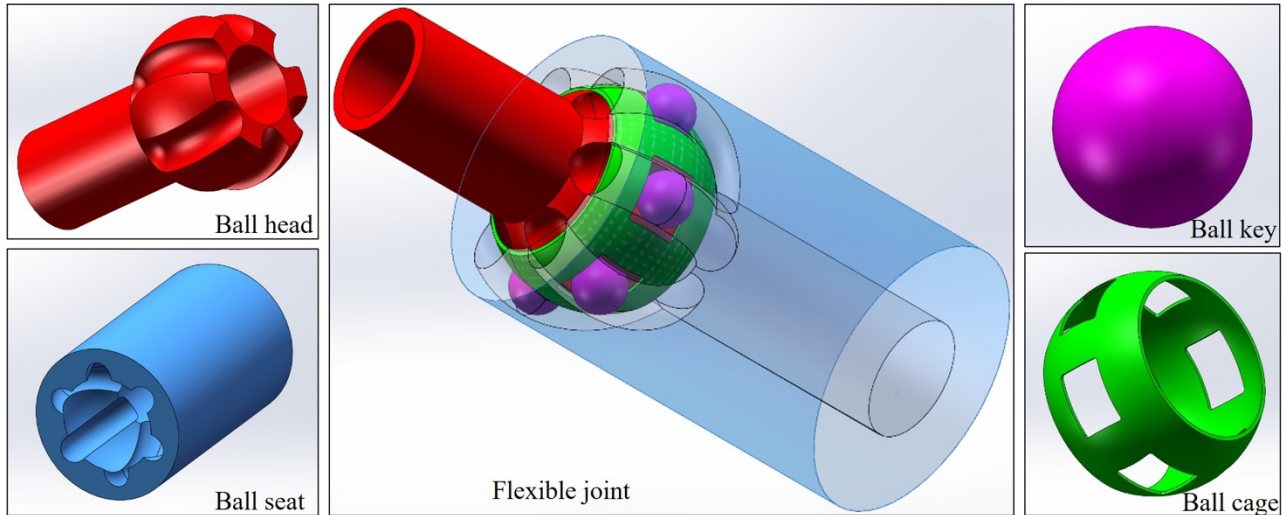


Fig. 4. Structure of flexible joint

Table 3 Material properties of flexible joint

Material parameters	Density	Young's Modulus	Poisson's Ratio	Shear Modulus	Yield Strength	Ultimate Strength
Value	7850 kg/m ³	2.1 GPa	0.3	8.1 GPa	835 MPa	980 MPa

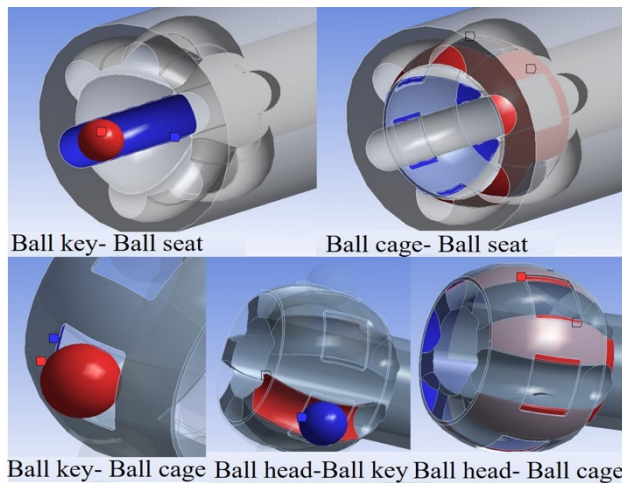


Fig. 5. The contact stress of each part of the flexible joint

The contact stress of each part was obtained at the deflection angles of 0°, 6°, 12°, and 18° (the maximum angle in the working process of the flexible joint). Fig. 6 shows the contact stress of the ball seat at the deflection angle of 0°. Fig. 7 shows the contact stress between the ball keys and ball seats. Fig. 6 and Fig. 7 show that under the action of axial force, the ball key is in contact with the center of the ball seat raceway, in which the maximum stress value of the ball seat is 940 MPa, and the maximum stress appears at the contact point between the 3# ball key and the ball seat. Due to the action of torque, the ball key will contact with the side of the ball seat raceway, and the stress contour of different ball keys and ball seats are roughly the same.

Notably, an obvious stress concentration is present at the contact point between the ball keys and ball seats.

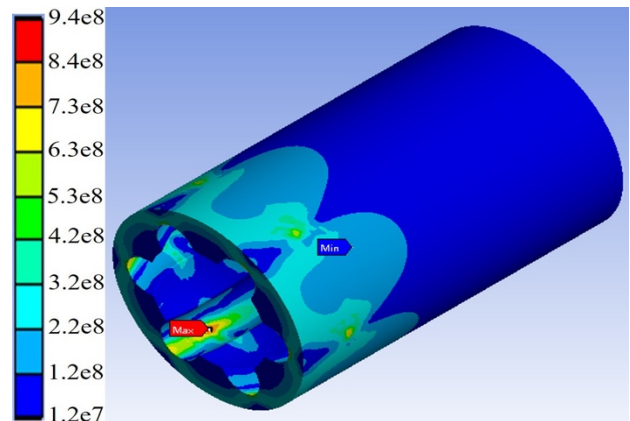


Fig. 6. The contact stress of ball seat

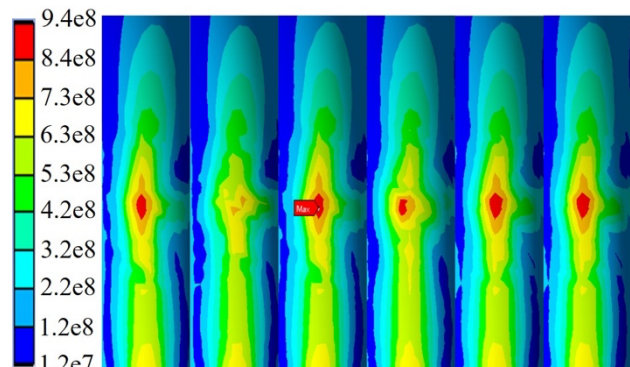


Fig. 7. The contact stress between ball key and ball seat

Fig. 8 shows the stress contour diagram of the ball head at the deflection angle of 0° , and Fig. 9 shows the contact stress contour diagram between different ball keys and the ball head. As shown in Fig. 8 and Fig. 9, the contact stress between the ball key and the raceway side of the ball head occurs under the action of torque, and an obvious stress concentration is present at the contact point between the ball key and ball head. The maximum stress value of the ball head is 2700 MPa at the contact point between the 6# ball key and the ball head.

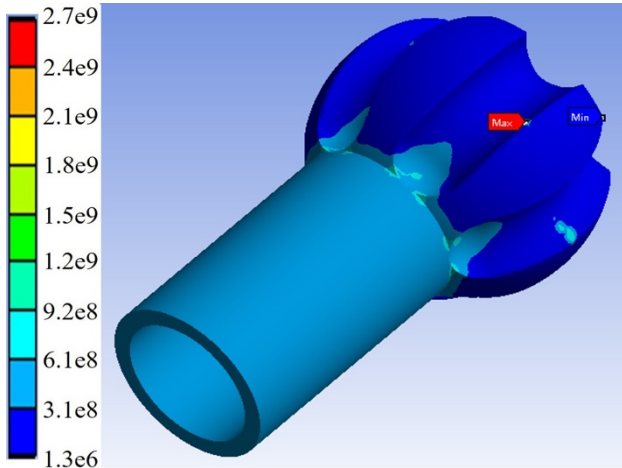


Fig. 8. The contact stress of ball head

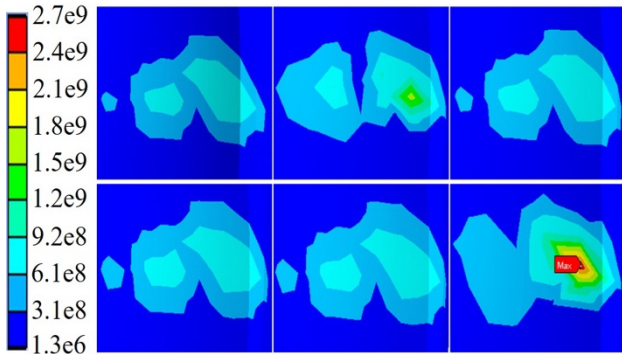


Fig. 9. The contact stress between ball key and ball head

Fig. 10 shows the stress of ball keys when the deflection angle is 0° , and Fig. 11 shows the contact stress contour of different ball keys and ball head. As shown in Fig. 10 and Fig. 11, the contact stress is obviously smaller than that between the ball key and the ball seat, and the maximum stress value between the ball key and the ball head is 1700 MPa. The maximum stress appears at the 2# ball key.

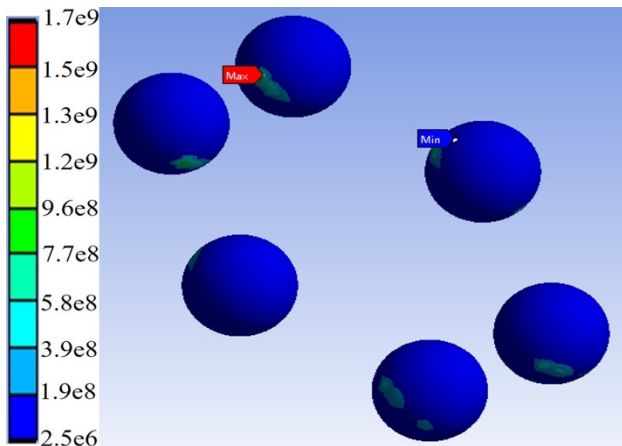


Fig. 10. The contact stress of ball key

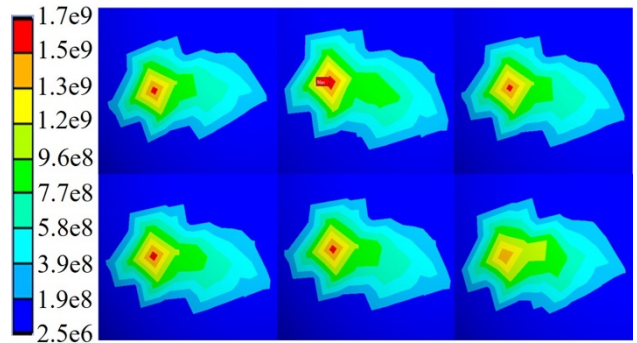


Fig. 11. The contact stress between ball head and ball key

Fig. 12 shows the contact stress of ball cage when the deflection angle is 0° . Fig. 13 and Fig. 14 show the contact stress of the ball cage with the ball seat and the ball head, respectively. The contact force between the ball cage, the ball seat and ball head are mainly friction, the contact stress produced are obviously less than that between other parts, and the distribution of contact stress is random. The maximum contact stress appears at the right angle of the ball cage window and the value is 650 MPa. Due to the ball cage window is square, stress concentration appears at the right angle.

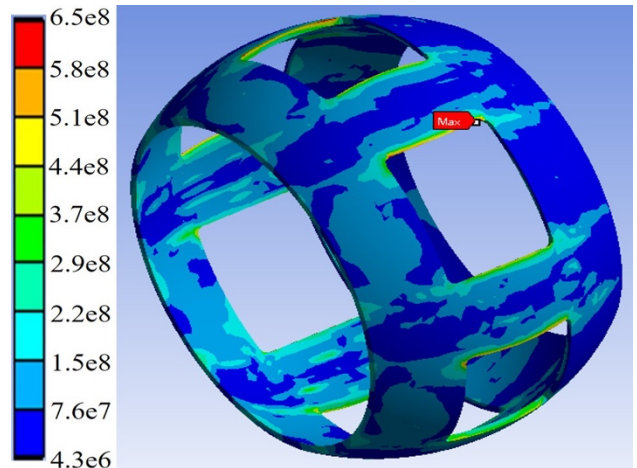


Fig. 12. The contact stress of ball cage

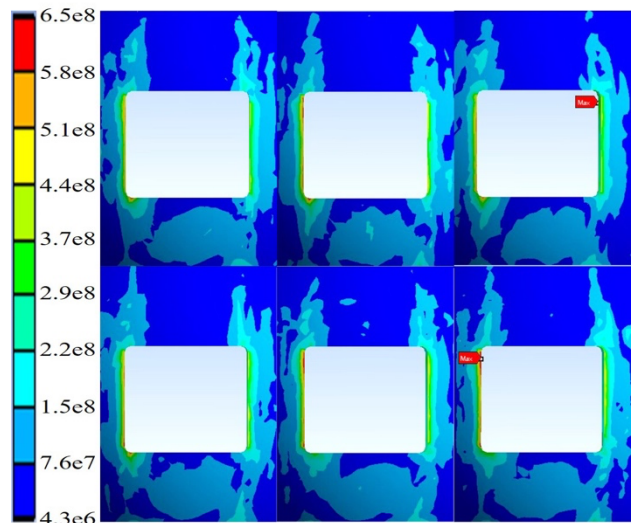


Fig. 13. The contact stress between ball seat and ball cage

Fig. 15 shows the contact stress curves of flexible joints with different deflection angles. A comparison of Fig. 6 with Fig. 15 showed an obvious stress concentration in the

contact parts among the ball key, ball head, and ball seat. The maximum contact stress increased with the increase in the deflection angle of the flexible joint. For the flexible joints with different deflection angles, the position where the maximum contact stress appears is random, but its value is less than the maximum contact stress obtained by Hertz theory. Among them, the contact stress of the ball key is higher and varies greatly with the deflection angle. Therefore, the ball key may be considered the most dangerous component of the flexible joint, and the diameter of the ball key can be appropriately increased to improve safety in practical engineering.

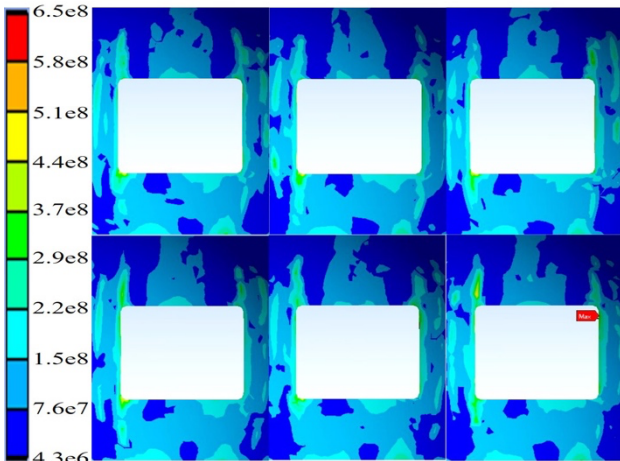


Fig. 14. The contact stress between ball head and ball cage

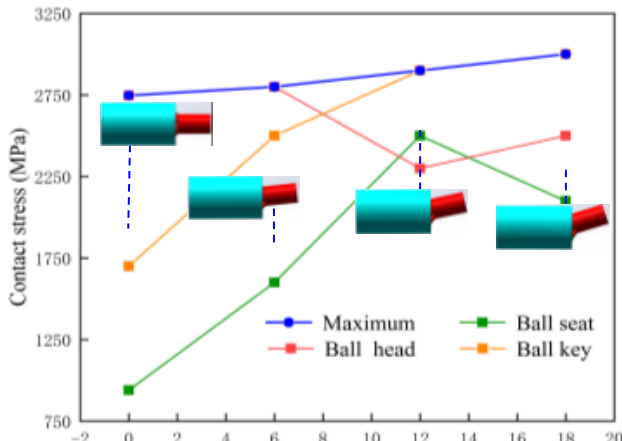


Fig. 15. Contact stress variation of flexible joints with different deflection angles

5. Conclusions

To explore the contact force characteristics of flexible joint, a novel analytical method for contact stress based on the classical Hertz theory was developed. The finite element method was used to study the variation of contact stress under the weight of bit and torque. The following conclusions could be drawn:

(1) Based on the Hertz contact theory, the maximum value of contact stress between the ball key and ball head is 4068.4 MPa, and the value between the ball key and ball seat is 4697.6 MPa.

(2) The contact stress values in the ball key, inner raceway, and outer raceway are concentrative. The maximum value of contact stress increases gradually with the increase in the deflection angle between the flexible joint.

(3) When the deflection angle between the flexible joint increases from 0 ° to 18 °, the contact stress increases to 220 MPa. However, the contact position is random on the inside of deflection.

(4) The contact stress of the ball key is the highest under drilling loads, and the variation range with the deflection angle is large. Therefore, the ball key is the most dangerous part of the flexible joint, and the contact stress can be reduced by increasing its diameter to ensure safety.

In this study, a novel analytical method for multibody collision contact stress on the flexible joint used in ultra-short-radius drilling tools is proposed. The results provide a reference for the parameter optimization of ball cage flexible joints. However, the contact force model will be modified in future studies to improve the calculation accuracy due to the lack of test data and field data in the current study.

Acknowledgements

This work was supported by the National Key Research and Development Program of China (No. 2019YFC1509204) and the Independent Innovation Research Program of China University of Petroleum (East China) (No.27RA2215005).

This is an Open Access article distributed under the terms of the Creative Commons Attribution License.



References

- Hill, G. J., Smith, Jr, H. G., Schnitker, M. W., Beatty, G. E., "Flexible Drill String Member Especially for Use in Directional Drilling". *US Patent US07/111222*, 14 March 1989.
- Luo, M., Xu, T. T., Jiang, J. J., Chi, X., Wang, J., Xue, S. H., "Two-layer Contact Nonlinear Mechanical Analysis of Flexible Drilling Tool in The Wellbore". *Computer Modeling in Engineering and Science*, 123(1), 2020, pp.75-100.
- Warren, T. M., Winters, W. J., Mount, H. B., Mason, K. L., "Short-Radius Lateral Drilling System". *Journal of Petroleum Technology*, 45(2), 1993, pp.108-115.
- Zhu, X. X., Xu, Y. P., Zhou, W. X., Ye, G. G., Zhou, B., "Research on Parameter Design Method and Motion Characteristics of a Ball Cage Flexible Joint". *Energies*, 15, 2022, pp.7591.
- Anoopnath, P. R., Babu, V. S., Vishwanath, A. K., "Hertz Contact Stress of Deep Groove Ball Bearing". *Materials Today-Proceedings*, 5(1) 2017, pp.3283-3288.
- Pandiyarajan, R., Starvin, M. S., Ganesh, K. C., "Contact Stress Distribution of Large Diameter Ball Bearing Using Hertzian Elliptical Contact Theory". *International Conference on Modelling Optimization and Computing*, 38, 2012, pp.364-269.
- Sharma, V., Patel, J., "Analysis of Contact Pressure for Inner and Outer Race of Ball Bearing 6004". *International Journal of Engineering Sciences & Research Technology*, 7(4), 2018, pp.287-292.
- Yousuf, L. S., Hadi, N. H., "Contact Stress Distribution of a Pear Cam Profile with Roller Follower Mechanism". *Chinese Journal of Mechanical Engineering*, 34(1), 2021. pp.266-279.
- Zhao, J. Z., Kan, Q. H., Fu, P. L., Kang, G. Z., Wang, P., "An Elasto-plastic Contact Solving Method for Two Spheres". *Acta Mechanica Sinica*, 33(5), 2020, pp.612-634.
- Derbew, M., Rao, D. N., Zeleke, E., "Modeling of braking thermal effect for wheel-rail contact parameters". *Proceedings of the Institution of Mechanical Engineers, Part F. Journal of Rail and Rapid Transit*, 235(8), 2020, pp.957-968.

11. Luo, M., Xu, T. T., Wang, J., Li, Q. Z., Zhang, J. H., "Contact nonlinear finite element analysis of controllable universal joint flexible slender in tube". *Journal of China University of Petroleum. Edition of Natural Science*, 43 (4), 2019, pp.75-81.
12. Xu, T. T., Luo, M., Jiang, J. J., Wang, J., Zhang, J. H., "Two-layer contact nonlinear mechanical analysis of controllable universal joint flexible structure in the tubes". *China mechanical engineering*, 15(31), 2020, pp.1798-1807.
13. Manzoli, O. L., Tosati, M., Rodrigues, E. A., Bitencourt, L. A. G., "Computational modeling of 2D frictional contact problems based on the use of coupling finite elements and combined contact/friction damage constitutive model". *Finite Elements in Analysis and Design*, 199(FEB.), 2022, pp.103658.1-103658.23.
14. Liu, Q., Tong, K., Zhu, G. C., Tan, Y., Zhang, J. T., Xu, X., Li, X. J., Song, S. Y., "Investigation of fracture causes of the titanium alloy drill pipe in ultra-short radius horizontal well drilling". *Engineering Failure Analysis*, 140, 2022, pp.106516.
15. Kui, Z., Lu, Y. J., Wei, W., Xia, A. F., "Parametric Design of Ball-cage Constant Velocity Joint Based on CATIA Customized Development". In: *The 3rd World Conference on Mechanical Engineering and Intelligent Manufacturing*, Shanghai, China: IEEE, 2020, pp.443-448.
16. Villamil, A. A. B., Casas-Rodriguez, J. P., Holguin, A. P., Barrera, M. S., "Mode I Crack Propagation Experimental Analysis of Adhesive Bonded Joints Comprising Glass Fibre Composite Material under Impact and Constant Amplitude Fatigue Loading". *Materials*, 14(16), 2021, pp.4380.
17. Marter, P., Daniel, C., Duvigneau, F., Woschke, E., "Numerical Analysis Based on a Multi-Body Simulation for a Plunging Type Constant Velocity Joint". *Applied Sciences*, 10(11), 2020, pp.3715.
18. Fischer, I. S., "Inertia dynamics of the Myard RCRCR constant-velocity coupling". *Mechanics Based Design of Structures and Machines*, 48(1), 2019, pp.68-86.
19. Simpson, M., Dolatabadi, N., Morris, N., Rahmani, R., Jones, D., "Analysis of a cross groove constant velocity joint mechanism designed for high performance racing conditions". *Proceedings of the Institution of Mechanical Engineers Part K-Journal of Multi-Body Dynamics*, 2022, pp.1-18.
20. Liang, H. W. R., Lee, C. K., Hui, S. Y. R., "Design, Analysis, and Experimental Verification of a Ball-Joint Structure with Constant Coupling for Capacitive Wireless Power Transfer". *IEEE Journal of Emerging and Selected Topics in Power Electronics*, 8(4), 2020, pp.3592-3591.